Improvement of the fracture toughness of hydroxyapatite (HAp) by incorporation of carboxyl functionalized single walled carbon nanotubes (CfSWCNTs) and nylon.

S. P. Khanal [a], H. Mahfuz [b], A. J. Rondinone [c], Th. Leventouri [a]

[a] Department of Physics, Florida Atlantic University, Boca Raton, FL 33431

[b] Department of Ocean and Mechanical Engineering, Florida Atlantic University, Boca Raton, FL 33431

[c] Center for Nanophase Materials Sciences, Oak Ridge National Laboratory, Oak Ridge, TN 37831

Corresponding author: S. P. Khanal, 777 Glades Road, Florida Atlantic University, Department of Physics, Boca Raton, FL 33431, Email address: skhanal2@fau.edu

Abstract

The potential of improving the fracture toughness of synthetic hydroxyapatite (HAp) by incorporating carboxyl functionalized single walled carbon nanotubes (CfSWCNTs) and polymerized ε - caprolactam (nylon) was studied. A series of HAp samples with CfSWCNTs concentrations varying from 0 to 1.5 wt. %, without, and with nylon addition was prepared. X-ray diffraction (XRD), Scanning Electron Microscopy (SEM), and Transmission Electron Microscopy (TEM) were used to characterize the samples. The three point bending test was applied to measure the fracture toughness of the composites. A reproducible value of 3.6 ± 0.3 MPa.√m was found for samples containing 1 wt. % CfSWCNTs and nylon. This value is in the range of the cortical bone fracture toughness. Increase of the CfSWCNTs content results to decrease of the fracture toughness, and formation of secondary phases.

Key Words: Hydroxyapatite (HAp), Single walled carbon nanotubes (SWCNTs), Fracture toughness, Nanocomposites.

1. Introduction

Synthetic Hydroxyapatite (HAp) of chemical formula $Ca_5(PO_4)_3OH$ could be an excellent material for bone replacement in approximately half million surgical procedures for human bone tissue repair per year that take place in the US alone [1]. However, the advantage of the HAp chemical similarity with the mineral phase of bone is outweighed by its poor mechanical properties that prevent its bulk use in orthopedic implants. Reported values for fracture toughness of pure HAp are in the range 0.5–1 MPa.√m [2-9], while the corresponding values for cortical bone are found in the range of 2-6 MPa.√m, depending on the direction of applied load [10-15].

Publications on improving the mechanical properties of HAp include hydroxyapatite-zirconia, glass, carbon fibers, carbon nanotubes, silver particles reinforced HAp, HAp whiskers, ion substituted HAp, and nylon [16-28].

Carbon nanotubes (CNTs) and its composites with HAp have attracted researchers' interest [28, 29-33]. Regarding the mechanical properties, Osorio et al., who have reported a maximum fracture toughness of 2.47 MPa.√m by adding 0.5 wt. % CNTs in the HAp matrix [28], while Li et al. have found an increase of the fracture toughness from 0.32 to 2.40 MPa.√m with addition of 3 wt. % CNTs [29], and Balani et al. have found a 56% increase with the addition of 4 wt. % CNTs to a coating of HAp [30]. However, these reported values remain at the low end of the bone measured fracture toughness range.

It is also reported that polymer infiltration into porous hydroxyapatite would be advantageous in fabricating high-performance composites, because of the mechanical properties of various polymers [21, 34-39], and the similarity of polymers with the collagen protein of the bone. Note that protein collagen (a polymer), the organic phase of bone, plays a vital role on its mechanical properties [40-43, 44]. It is stated that infiltration of nylon (polymer) into a highly porous HAp increased its fracture toughness up to 1.65 MPa.√m [18], a value that is higher than the pure HAp ones, but still below the lower end of the bone range.

In an effort to further enhance the mechanical properties of HAp, we introduce carboxyl functionalized single walled carbon nanotubes (CfSWCNTs) and nylon in the preparation process of HAp. Here we report results of fracture toughness and work of fracture experiments from a series of samples that were characterized by X-ray diffraction (XRD), Scanning Electron Microscopy (SEM), and Transmission Electron Microscopy (TEM) equipped with Energy Dispersive X-Ray Spectroscopy (EDS).

2. Experimental

2.1 Synthesis of the samples

A series of samples was prepared by applying a modified in situ chemical precipitation method [45] using the starting materials: Ammonium phosphate dibasic (≥99.99%) $(NH_4)_2HPO_4$, calcium nitrate tetrahydrate (99.98%) $Ca(NO_3)_2.4H_2O$, COOH-functionalized single walled carbon nanotubes (CfSWCNTs) of diameter ~1.5 nm and length 1-5µm, ε - Caprolactam (monomer form of nylon), and 6-aminocaproic acid.

The samples were named S1, S2, S3, S4, S5, S6, S7 and S8 as in Table 1. The first sample S1 is pure HAp, S2, S3 and S4 are HAp containing 0.5, 1 and 1.5 wt. % CfSWCNTs correspondingly. The sample S5 consists of HAp and nylon. The samples S6, S7, and S8 consist of HAp, CfSWCNTs in wt. % of 0.5, 1, 1.5 correspondingly, and nylon.

Table 1. Prepared samples and corresponding compositions.

Sample Name	Sample Composition
S1	SHAp (Pure Hydroxyapatite)
S2	SHAp05SWCNT (Hydroxyapatite and 0.5 wt.% CfSWCNT)
S3	SHAp10SWCNT (Hydroxyapatite and 1 wt.% CfSWCNT)
S4	SHAp15SWCNT (Hydroxyapatite and 1.5 wt.% CfSWCNT)
S5	SHApNylon (Hydroxyapatite and Nylon)
S6	SHAp05SWCNTNylon (Hydroxyapatite, 0.5 wt.% CfSWCNT and Nylon)
S7	SHAp10SWCNTNylon (Hydroxyapatite, 1 wt.% CfSWCNT and Nylon)
S8	SHAp15SWCNTNylon (Hydroxyapatite, 1.5 wt.% CfSWCNT and Nylon)

Figure 1 is a schematic diagram of the preparation process of the samples; quantification of the chemicals applies to sample S2.

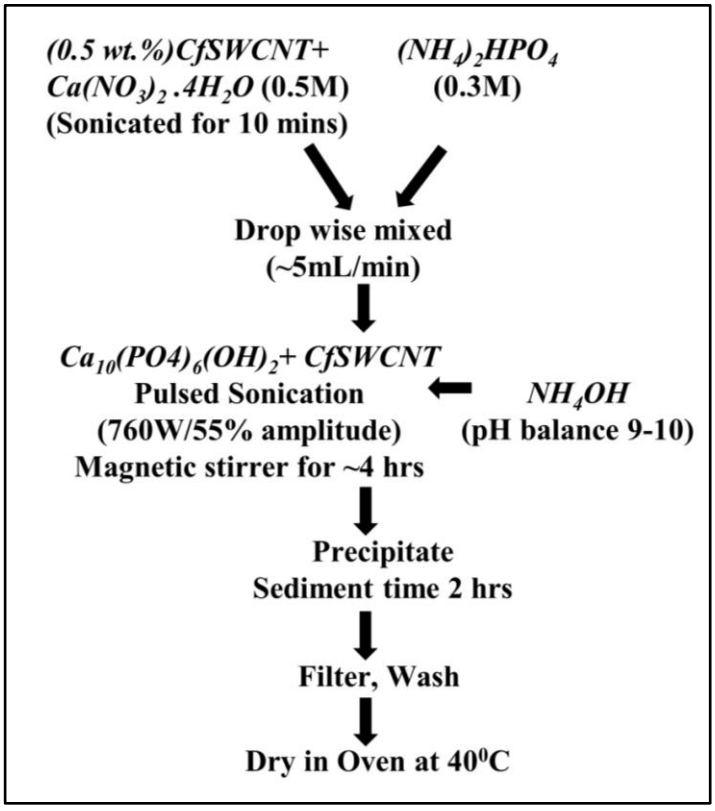

Fig. 1. Schematic diagram of synthesis of the (CfSWCNT)/HAp sample S2.

Briefly, a 0.5M of $Ca(NO_3)_2.4H_2O$ solution was prepared and 0.5 wt % of CfSWCNTs were added. Then, a 0.3M solution of $(NH_4)_2PO_4.4H_2O$ was added drop wise while a magnetic stirrer was used during the process. The pH was maintained in the range of 9-10 with the addition of NH_4OH during the sonication and precipitation processes. The ultrasonicator was set up in pulse mode (10 sec on and 10 sec off) and the final solution was sonicated for 10 mins. During the sonication and precipitation processes the temperature increased from 23°C to 42°C. The precipitated solution was filtered and washed 3 times with DI water, and dried in oven at 40°C.

The same process was followed in synthesis of the samples S3, S4 with addition of 1 and 1.5 wt. % CfSWCNTs correspondingly. Then, part of each of S1, S2, S3 and S4 was used to prepare the nylon containing composites S5, S6, S7, and S8. First, appropriate amount of ε-caprolactam was mixed in a beaker with water on a hot plate and 6-aminocaproic acid to initiate polymerization. Then the sieved powder of each one of the S1, S2, S3, S4 was mixed in the melted polymerized solution and stirred on a hot plate until the powder was uniformly distributed (hot blending). The solution was then quenched on a steel plate and part of it was poured into a mold to make a block for the three point bending test.

2.2 Characterization methods

Powder x-ray diffraction patterns were collected using a SIEMENS D5000 diffractometer operating at 45 kV and 40 mA with Cu K_α radiation and a diffracted beam monochromator. Data were collected in the 2θ range of 8°-90° with a step size of 0.02° and counting time of 12 sec at each step. The data bank from the International Center for Diffraction Data (ICDD) was used in a search/match program for phase identification. The Rietveld refinement method [46] in the GSAS program [47,48] was used for crystal structure analysis of the diffraction patterns of S1, S2, S3 and S4.

Size, morphology and chemical analysis of the crystallites in the samples were studied using a Zeiss LIBRA 120 PLUS Transmission Electron Microscope equipped with EDS (Energy Dispersive x-ray Spectroscopy) and an in-column Omega filter, operating at 120 kV. SEM images were collected using a Zeiss Orion NanoFab electron microscope.

Fracture toughness is a measure of a material's ability to resist fracture in the presence of a crack. The tests generally require a specimen that contains a pre-existing crack. The three point bending test was performed to measure the mode 1 critical stress intensity factor (fracture toughness K_{1C}) of the samples using a VC 750 and Zwick/Roell Z050, in compliance with the ASTM D 5045 standard [49].The following equation was used in order to calculate K_{1C}.

$$K_Q = \left[\frac{P_Q}{B \times W^{1/2}} \right] f(x) \tag{1}$$

where K_Q is the conditional critical stress intensity factor, x = α/W, W is the height of the specimen, α is the pre-cracked length, P_Q is the critical load, B is the specimen's width. The stress intensity shape factor $f(x)$ is found from the equation:

$$f(x) = 6x^2 \frac{\left[1.99 - x(1-x)(2.15 - 3.93x + 2.7x^2)\right]}{(1+2x)(1-x)^{3/2}} \tag{2}$$

$K_Q = K_{1C}$ under the condition:

$$B, \alpha, (W - \alpha) > 2.5 \left(\frac{K_Q}{\sigma_y} \right)^2 \tag{3}$$

where σ_y in equation (3) is the yield stress.

The dimensions, $B \times W \times S \times L$, of the block specimens was 4×8×32×36 in mm where S is the distance between the supporting points (*span*).

A diamond wheel of thickness 0.1mm was used to make the pre-crack α on the block where α is ~W/2 mm. The speed of the cross head was set at 10 mm/min during the fracture

toughness testing. Three similar blocks were made from each category of samples S1-S8 to test the reproducibility of fracture toughness. The blocks S1 through S4 were sintered at 400°C for about 12 hours in a furnace, while S5-S8 were not sintered because of the nylon. The value of the critical load P_Q of the equation (1) for each sample was found from the load displacement (L-D) measurements.

The fracture resistant parameter or work of fracture was calculated from the L-D data. The work of fracture is defined by the ratio of the area covered by the load displacement (L-D) curve to the cross-section $W \times B$ of the block [50].

3. Results and discussion

3.1 XRD studies

Hydroxyapatite (ICDD PDF2 # 09-432) was identified as the main phase in all samples. The XRD patterns of S1-S4 of Fig. 2 show a well-crystallized material that becomes less crystallized as the CfSWCNTs content increases. A single HAp phase was identified in the samples S1, S2 and S3. Brushite ($CaHPO_4.2H_2O$, ICDD PDF2 # 72-0713) was identified as a secondary phase in the sample S4. The major Carbon peak (ICDD PDF2 # 41-1487, $2\theta=26.382^o$) was identified only in sample S4, because of the small amounts in S2, S3 that are below detection limits of the diffractometer. It is shown in the inset of Fig. 2.

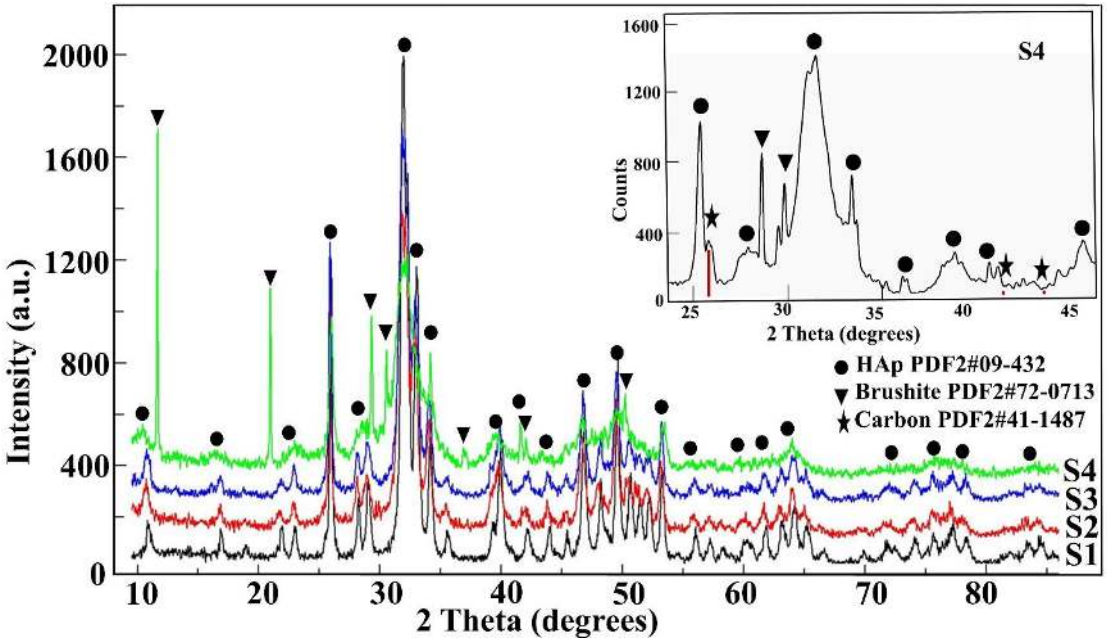

Fig. 2. Phase identification of the diffraction patterns collected from the samples S1, S2, S3, S4. The major peaks of carbon identified in sample S4 are marked with asterisks in the inset.

When nylon is added in the processing, the diffraction peaks broaden, indicating less crystallized material, while nylon and ε - Caprolactam peaks appear as shown in Fig. 3 for the case of sample S7.

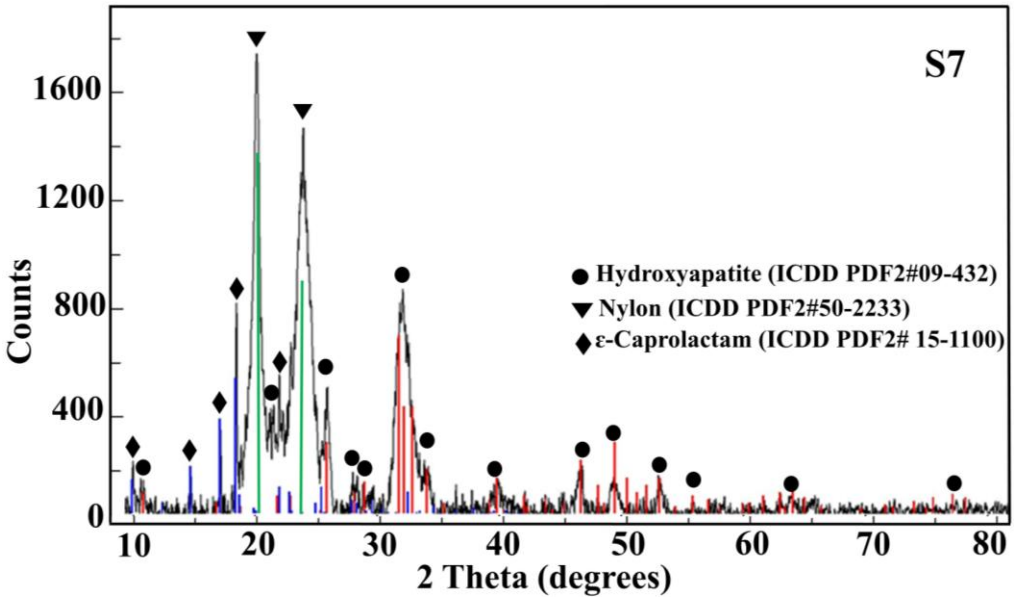

Fig. 3. Phase identification of the diffraction pattern collected from the sample S7.

The particle size was calculated from the FWHM of the main HAp Bragg peak (211) using the Scherrer equation $\tau = K\lambda/\beta\cos\theta$ (K=0.9, assuming spherical particles). Fig. 4 illustrates the effect of CfSWCNTs concentration on the particle size in samples S1-S4. Data from the diffraction patterns of the samples S5 to S8 are not included in Fig. 4, because of the broadening and overlapping of the Bragg peaks in those patterns, due to addition of nylon.

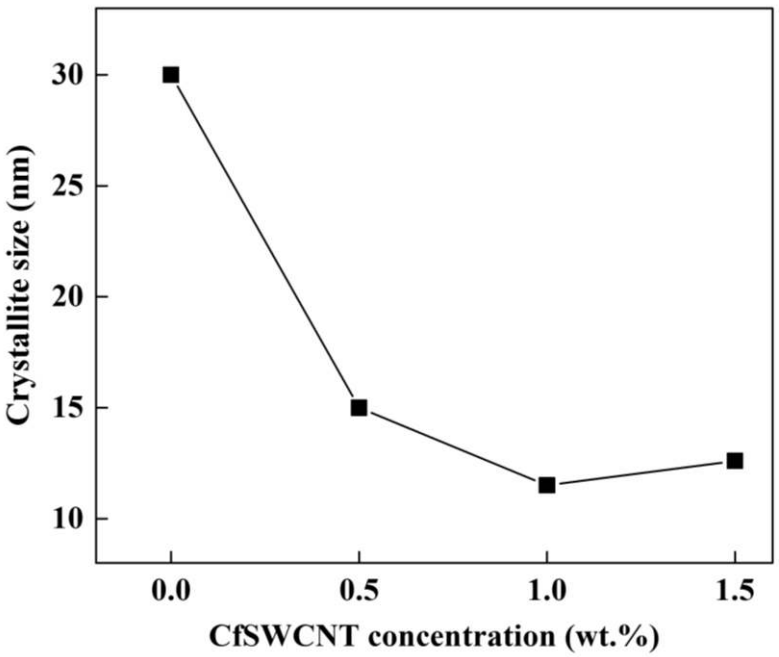

Fig. 4. Crystallite size of the samples S1-S4 versus the CfSWCNT concentration.

Peak broadening and amorphous phases did not allow for Rietveld refinement of the diffraction patterns of the samples S5-S8. The HAp phase in space group P63/m with isotropic atomic displacement parameters was introduced in the calculated pattern of the samples S1, S2, and S3[51]. The monoclinic brushite phase, space group I1a1, was added in the refinement of the pattern of S4 to account for the secondary identified phase. Fig. 5 shows an example of refinement from the diffraction pattern of sample S3.

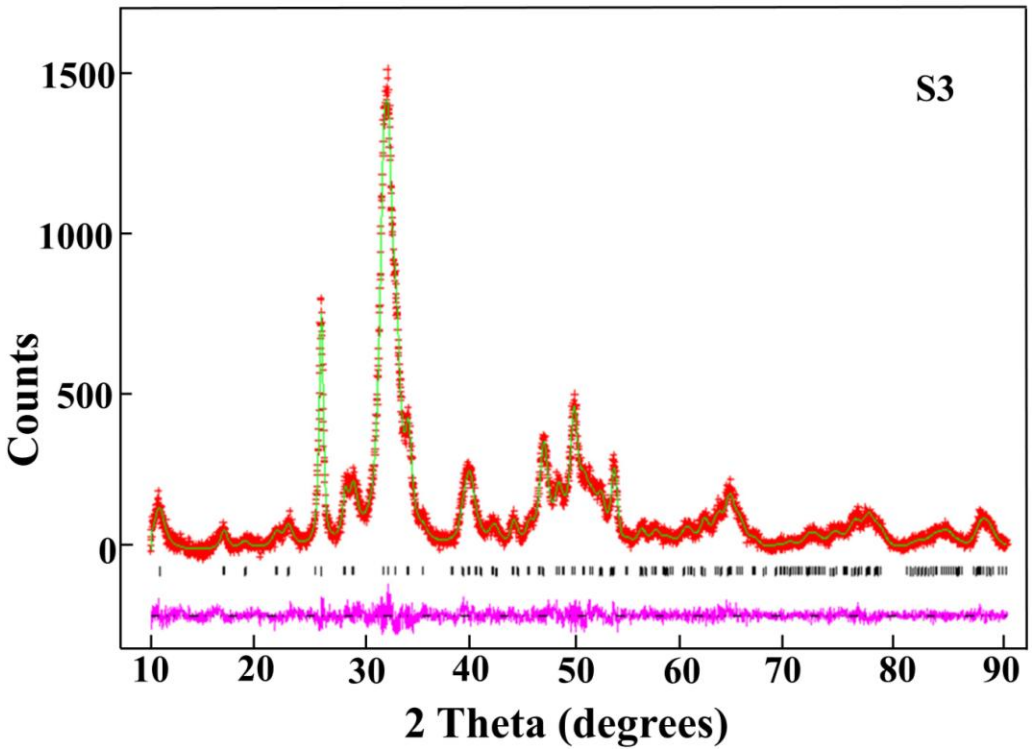

Fig. 5. Rietveld refinement of the diffraction pattern of sample S3. Red crosses mark the experimental pattern and the green line is the calculated pattern. The black vertical lines mark the HAp Bragg diffraction peaks and the magenta line is the difference between the experimental and refined patterns.

Refined lattice constants, weighted pattern residuals, the ratios of the refined site occupancies of the Ca and P atoms, and the interplanar distances of the major HAp peak (211), and the (002) are listed in Table 2. No systematic change in the lattice constants is observed as the CfSWCNT concentration increases from 0 to 1.5 wt. % in samples S1-S4. The small non-systematic variations in the lattice constants, and small changes in the interplanar spaces could be attributed to the processing of the samples. The noticeable decrease of the Ca/P ratio in sample S4 is justified by the formation of 18.36 wt.% brushite ($CaHPO_4.2H_2O$).

Table 2. Rietveld refined parameters, d_{211} and d_{002} from the diffraction patterns of S1, S2, S3, S4.

Sample Name	Identified Phases	a (Å)	c (Å)	R_{wp}	χ^2	Ca/P	d_{211} (Å)	d_{002} (Å)
S1	HAp	9.4466(7)	6.8870(4)	0.08	1.30	1.64	2.8208(2)	3.4435(5)
S2	HAp	9.4443(3)	6.8901(2)	0.08	1.47	1.60	2.8205(1)	3.4450(2)
S3	HAp	9.4547(7)	6.8893(4)	0.07	1.18	1.68	2.8231(2)	3.4460(5)
S4	HAp 81.64%	9.4683(1)	6.8737(6)	0.11	2.68	1.54	2.8242(3)	3.4368(3)
	Brushite 18.36%							

3.2 Electron microscopy studies

Homogeneity in particle size and shape is observed in the SEM image from sample S1 (pure HAp) of Figure 6a. When CfSWCNTs are added, the homogeneity is reduced in samples S2, and S4 as the images b and c show correspondingly.

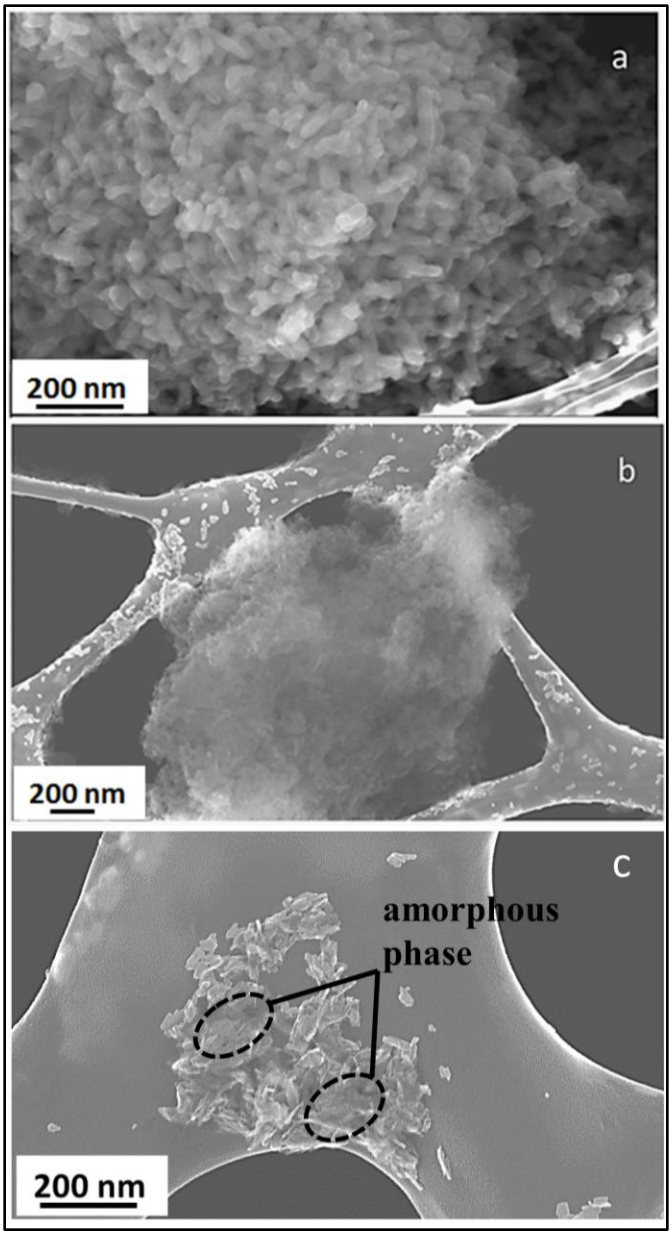

Fig. 6. SEM images from the samples S1, S2 and S4 (a-c correspondingly).

TEM images collected from the samples S1-S4 are shown in Fig. 7. Morphology of the HAp crystallites and CNTs is revealed (Fig. 7b), as well as broken and agglomerated CNTs in sample S4 (Fig. 7d). The particle size varies from ~30-70 nm. Notice that the image from sample S3 displays the most uniform distribution of carbon nanotubes in the HAp matrix, which is probably

one of the factors leading to a composite with better mechanical properties. EDS has confirmed the presence of the atoms in the HAp crystallites, carbon nanotubes and nylon.

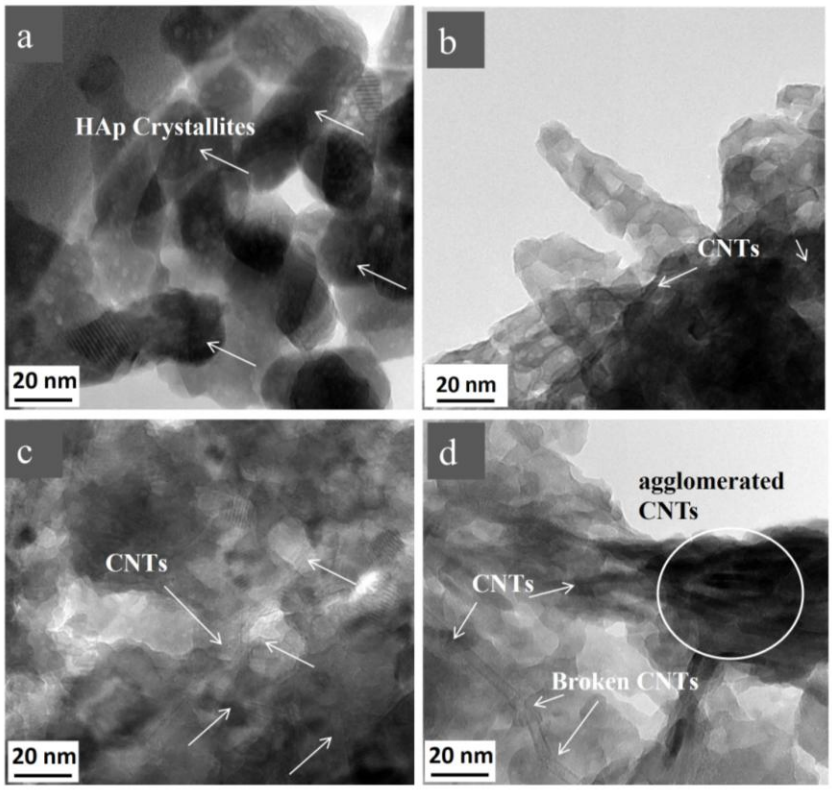

Fig. 7. TEM images from the samples S1-S4. Images b, c, and d display the CNT distribution in the HAp phase.

Figure 8 shows TEM images of the COOH- functionalized single walled carbon nanotubes (CfSWCNTs) used in this study. Entangled, broken, as well as multi-walled carbon nanotubes are illustrated in this figure.

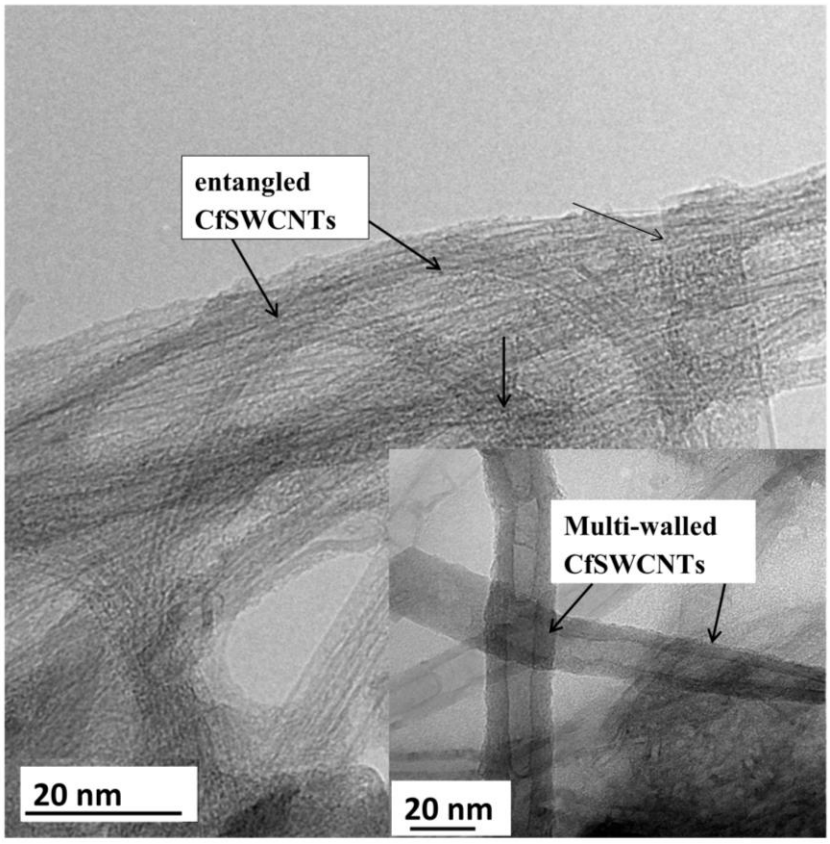

Fig. 8. TEM images of the COOH- functionalized single walled carbon Nanotubes (CfSWCNTs) used in this study. Multi-walled carbon nanotubes are also shown in the inset.

SEM images from sample S7 (1% wt. CfSWCNTs and nylon) of Fig. 9 display an amorphous nylon, and a non-homogenous crystallite distribution over the nylon surface. Images from the other samples containing nylon (S5, S6, S8) are not shown because of the images' poor quality.

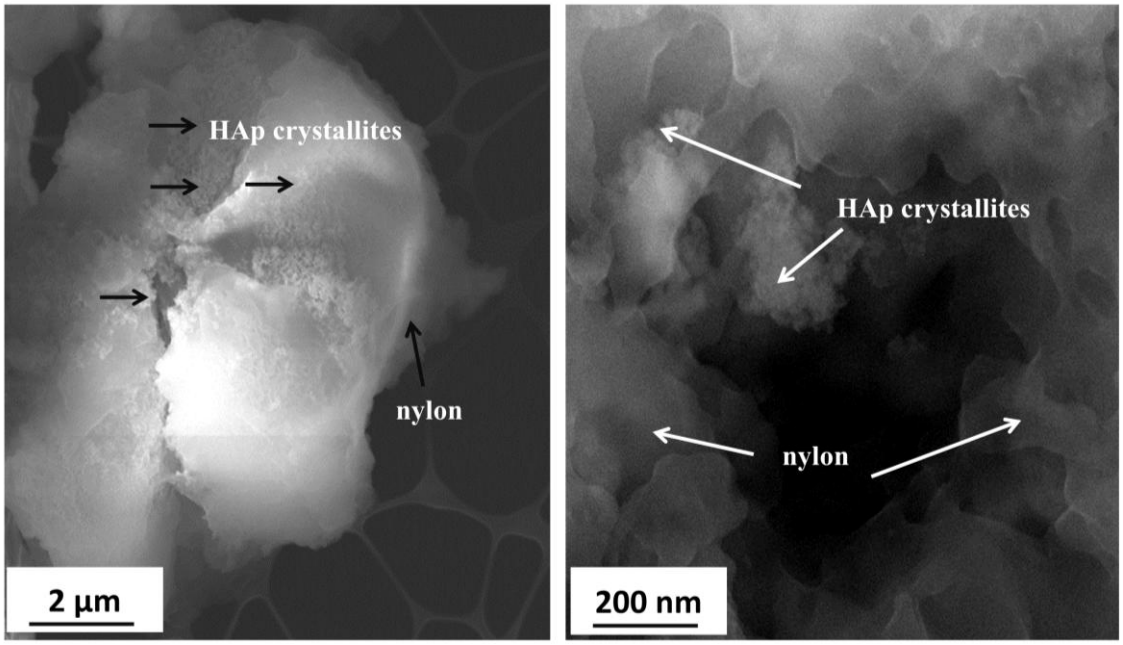

Fig. 9. SEM images taken from the sample S7 (HAp, 1 wt. % CfSWCNTs and nylon).

3.3 Mechanical properties

The average values of fracture toughness, as found from measurements of three samples from each type S1-S8, along with their standard deviations are plotted in Fig. 10. The highest fracture toughness (3.6 ± 0.3 MPa.√m) was found for the sample S7 that contains 1wt. % CfSWCNTs and nylon. Keep in mind that the sample S7 was prepared with addition of nylon in S3, which displayed the highest uniformity in CNTs distribution (Fig. 7c).

To our knowledge, value comparable to the published ones for cortical bone, is reported for the first time for composite HAp. A possible mechanism for such improvement of the fracture toughness of synthetic HAp could be a combination of several factors: The functionalization and sonication in the preparation process promote homogeneous dispersion of CNTs in the HAp matrix, then the negatively charged carboxyl functional groups (-COOH) of the carbon nanotubes attract the Ca^{2+} ions and form bonds between HAp and carbon nanotubes [52], functionalization

weakens the van der Waals forces between the SWCNTs, facilitates the hydrogen bonding between nanotubes and the HAp matrix reinforcing the CfSWCNTs-HAp interface, while the highly porous HAp ease nylon penetration into its matrix. Each one of these factors is separately reported to improve the mechanical properties of hydroxyapatite [18,53, 54, 55]. In our studies, it seems that combination of good dispersion of CfSWCNTs, and strong interfacial bonding facilitated by nylon, results to higher values of fracture toughness.

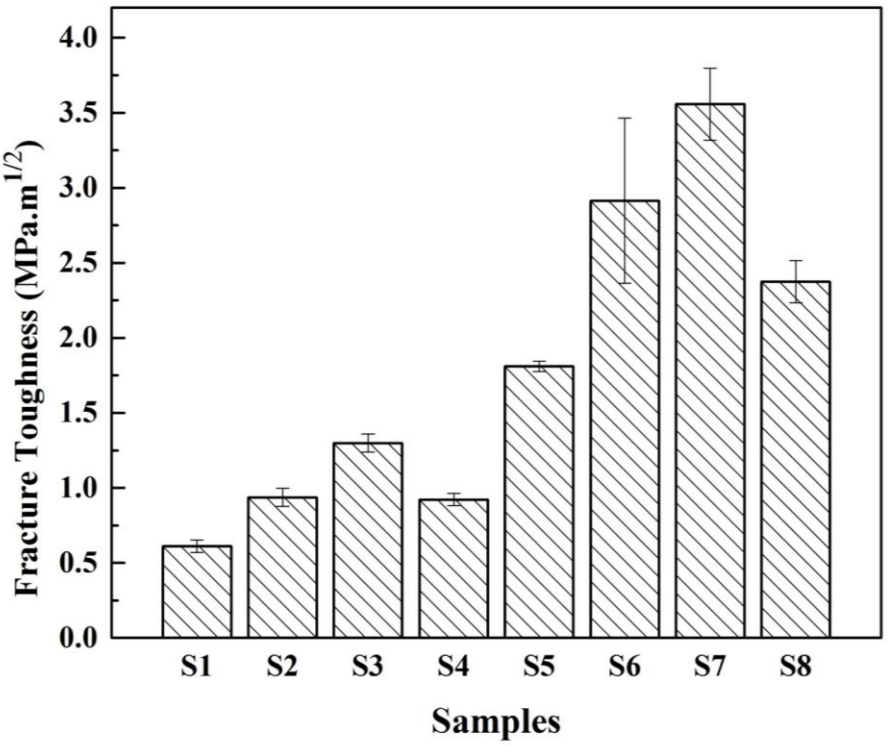

Fig. 10. The fracture toughness of samples S1-S8.

Additional supporting evidence of the proposed mechanism for the improved fracture toughness of synthetic HAp comes from the load versus displacement (L-D) plot for the representative samples of this study S1, S3, S7 and S8 of Fig. 11. The corresponding values of the

work of fracture are: 108, 183, 644 and 310 J/m^2. The highest work of fracture for the sample S7 indicates that the crack propagating through the HAp is restricted by the incorporation of CNTs and nylon. The values for S7 and S8 are significantly higher from those measured for HAp/Nylon-6, as well as for bovine femur [56]. In addition, the fracture propagation in sample S7 and S8 ended in catastrophic failure compared to the S1 and S3 specimens, which indicates primarily adhesive bonding between nylon and HAp-CfSWCNTs.

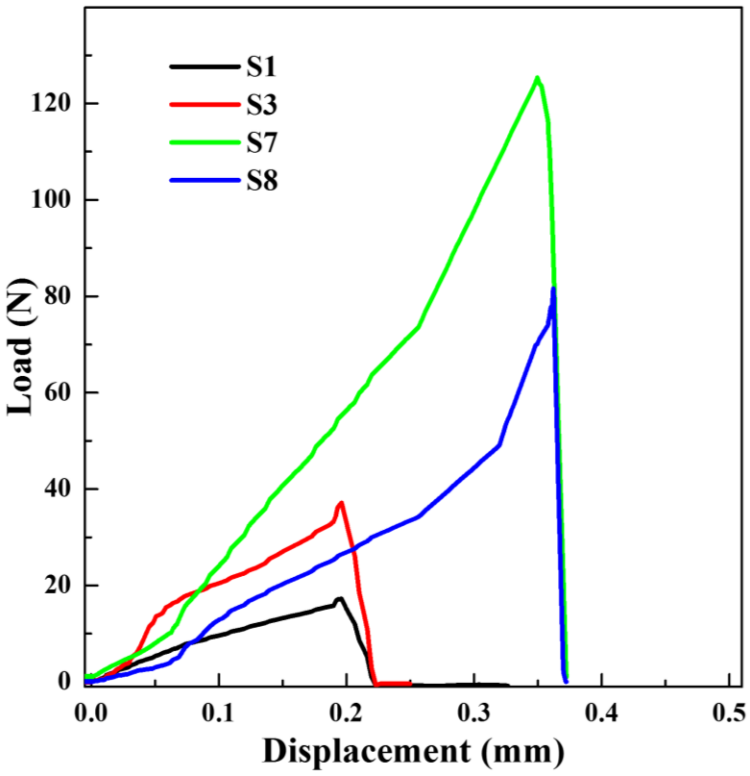

Fig. 11. The load-displacement (L-D) curve of the samples S1, S3, S7 and S8.

When the CfSWCNTs concentration increases above 1 wt. %, the agglomeration of CfSWCNTs (Fig. 7d) affects unfavorably the energetics of the system and prevents further infiltration in the HAp porous structure. In addition to agglomeration, development of the brushite secondary phase probably does not help the mechanical performance of the composites.

4. Conclusions

This research has shown that incorporation of CfSWCNTs and nylon in synthetic hydroxyapatite results to increased fracture toughness up to a reproducible maximum value of 3.60 MPa.√m, and 644 J/m^2 work of fracture for samples containing 1 wt. % CfSWCNTs and nylon. Addition of nylon was critical in achieving such values that are comparable to the ones of the cortical bone. Increase of the CfSWCNTs content above 1 wt. % results to decrease of the fracture toughness and work of fracture, loss of crystallinity, and formation of secondary phases.

Acknowledgements

Part of this research was conducted at the Center for Nanophase Materials Sciences, which is sponsored at Oak Ridge National Laboratory by the Scientific User Facilities Division, Office of Basic Energy Sciences, U.S. Department of Energy. Support from FAU with a *Dissertation of the Year Award* to the first author is gratefully acknowledged.

References

[1] M. Geiger, R.H. Li, W. Friess

Collagen sponges for bone regeneration with rhBMP-2

Adv. Drug. Deliv. Rev., 55 (2003), pp. 1613-1629

[2] M. Akao, H. Aoki, K. Kato

Mechanical properties of sintered hydroxyapatite for prosthetic applications

J. Mat. Sci., 16 (1981), pp. 809-812

[3] K.A. Hing, S.M. Best, W. Bonfield

Characterization of porous hydroxyapatite

J. Mat. Sci.: Mat. in Med., 10 (1999), pp. 135-145

[4] M. Jarcho, C.H. Bolen, M.B. Thomas, J. Bobick. J.F. Kay, R.H. Doremus

Hydroxyapatite synthesis and characterization in dense form

J. Mat. Res., 11 (1976), pp. 2027-2035

[5] P.E. Wang, T.K. Chaki

Sintering Behavior and Mechanical-Properties of Hydroxyapatite and Dicalcium Phosphate

J Mat. Sci., 4 (1993), pp. 150-158

[6] A. A. White, S.M. Best, I. A. Kinloch

Hydroxyapatite and carbon nanotube composites for biomedical applications

Inter. J. App. Cer. Tech., 4 (2007), pp. 1-13

[7] P. Van Anduyt, F. Li, J.P. Keustermans, J.M. Streydio

The influence of high sintering temperatures on the mechanical properties of hydroxyapatite

J. Mat. Sci., 6 (1995), pp. 8-13

[8] G. De With, H.J. A. Van Dijk , N. Hattu, K. Prijs

Preparation, microstructure and mechanical properties of dense polycrystalline hydroxyapatite

J. Mat. Sci., 16 (1981), pp. 1592-1598

[9] S.V. Dorozhkin

Bioceramics based on calcium orthophosphates

Glass Ceram., 64 (2007) pp. 442-447

[10] R.B. Ashman, S.C. Cowin, W.C. Van Buskirk, J.C. Rice

A Continuous Wave Technique for the Measurement of the Elastic Properties of Cortical Bone

J Biomechs., 17: (1984), pp. 349-361

[11] X.E. Guo

Mechanical Properties of Cortical Bone and Cancellous Bone Tissue

Bone Mechanics Handbook, Ed SC Cowin, Boca Raton, FL: CRC, (2001), pp 10.1-10.23

[12] R.K. Nalla, J.S. Stölken, J.H. Kinney, R.O. Ritchie

Fracture in Human Cortical Bone: Local Fracture Criteria and Toughening Mechanisms

J. Biomechs., 38 (2005), pp. 1517-1525

[13] R.B. Martin, D.B. Burr, N.A. Sharkey

Skeletal Tissue Mechanics

New York Springer(1998) ISBN: 0-387-98474-7

[14] J.Y. Rho, L. Kuhn-Spearing, P. Zioupos

Mechanical Properties and the Hierarchical Structure of Bone

Med. Eng. Phys. 20 (1998), pp. 92-102

[15] D.T. Reilly, A.H. Burstein

The Elastic and Ultimate Properties of Compact Bone Tissue

J. Biomech., 8 (1975), pp. 393-405

[16] B. Bracci, P. Torricelli, S. Panzavolta, E. Boanini, R.Giardino, A. Bigi

Effect of $Mg^{2+,}$ Sr^{2+}, and Mn^{2+} on the Chemico-Physical and in Vitro Biological Properties of Calcium Phosphate Biomimetic Coatings

J. Inorg. Biochem. 103 (2009), pp. 1666-1674

[17] S. Okayama, M. Akao, S. Nakamura S, Y. Shin, M. Higashikata. H. Aoki

The mechanical properties and solubility of strontium-substituted hydroxyapatite

Biomed. Mat. Eng., 1 (1991), pp. 11-17

[18] A. Nakahira, M. Tamal, S. Miki, G. Pezzotti

Fracture behavior and biocompatibility evaluation of nylon-infiltrated porous hydroxyapatite

J. Mat. Sci., 37 (2002), pp. 4425-4430

[19] K.S. TenHuisen, R.I. Martin, M. Klimkiewicz, P.W. Brown

Formation and properties of a synthetic bone composite: Hydroxyapatite–collagen

J. Biom. Mat. Res., 29 (1995), pp. 803-810

[20] G. Wenmin, Z. Yihe, Z. Wei

Mechanical properties and crystallization behavior of hydroxyapatite/poly(butylenes succinate) composites

J. Biom. Mat. Res., 101 (2013), pp. 2500-2506

[21] G. Wei, P.X. Ma

Structure and properties of nano-hydroxyapatite/polymer composite scaffolds for bone tissue engineering

Biomaterials, 25 (2004), pp. 4749-4757

[22] C.T. White, J.W. Mintmire

Fundamental Properties of Single-Wall Carbon Nanotubes

J. Phys. Chem., B 109 (2005), pp. 52-65

[23] Z.J. Shen, E. Adolfsson, M. Nygren, L. Gao, H. Kawaoka, K. Niihara

Dense hydroxyapatite-zirconia ceramic composites with high strength or biological applications

Adv. Mat., 13 (2001), pp. 214-216

[24] F.N. Oktar, G. Göller

Sintering effects on mechanical properties of glass-reinforced hydroxyapatite composites

Ceram. Int., 28 (2002), pp. 617-621

[25] X. Zhang, G.H.M. Gubbels, R.A. Terpstra, R. Metselaar

Toughening of calcium hydroxyapatite with silver particles

J. Mat. Sci., 32 (1997), pp. 235-43

[26] K. Park, T. Vasilos

Characteristics of carbon fibre-reinforced calcium phosphate composites fabricated by hot pressing

J. Mat. Sci. Lett., 16 (1997), pp. 985-987

[27] W. Suchanek, M. Yashima, M. Kakihana, M. Yoshimura

Hydroxyapatite/hydroxyapatite -whisker composites without sintering additives: mechanical properties and microstructural evolution

J. Am. Ceram. Soc., 80 (1997), pp. 2805-2813

[28] A.G. Osorio, L.A. dos Santos, C.P. Bergmann

Evaluation of the mechanical properties and microstructure of hydroxyapatite reinforced with carbon

Rev. Adv. Mat. Sci., 27 (2011), pp. 58-63

[29] A.M. Li, K.N. Sun, W.F. Dong, D. Zhao

Mechanical properties, microstructure and histocompatibility of MWCNTs/HAp biocomposites

Mat. Lett., 61 (2007), pp. 1839-1844

[30] K. Balani, R. Anderson, T. Laha, M. Andara, J. Tercero, E. Crumpler, A. Agrawal

Plasma-sprayed carbon nanotube reinforced hydroxyapatite coatings and their interaction with human osteoblasts in vitro

Biomaterials, 28 (2007), pp. 618-24

[31] H. Zanin, P. W. May, A. O. Lobo, E. Saito, J. P. B. Machado, G. Martins, V. J. Trava-Airoldi, E. J. Corat

Effect of Multi-Walled Carbon Nanotubes Incorporation on the Structure, Optical and Electrochemical Properties of Diamond-Like Carbon Thin Films

J. Electrochem. Soc., 161 (2014), pp. H290-H295

[32] I.A. Siqueira, C. A. Oliveira, H. Zanin, M.A. Grinet , A.E. Granato, M.A. Porcionatto, F. R. Marciano, A.O. Lobo

Bioactivity behavior of nano-hydroxyapatite/freestanding aligned carbon nanotube oxide composite

J. Mater. Sci. Mater. Med., 26 (2015), pp.113

[33] H. Zanin, C. M. R. Rosa, N. Eliaz, P. W. May, F. R. Marcianoa A. O. Lobo
Assisted deposition of nano-hydroxyapatite onto exfoliated carbon nanotube oxide scaffolds
Nanoscale, 7 (2015), pp. 10218-10232

[34] W. Bonfield, M.D. Grynpas, A.E. Tully, J. Bowman, J. Abram
Hydroxyapatite Reinforced Polyethylene-A Mechanically Compatible Implant Material for Bone Replacement
Biomaterials, 2 (1981), pp. 185-186

[35] T.P.T. Ton, K.E. Tanner, W. Bonfield
Fatigue Characterization of a Hydroxyapatite-Reinforced Polyethylene Composite. I. Uniaxial Fatigue
J. Biomed. Mat. Res. 51 (2000), pp. 453-460

[36] E. Tayton, M. Purcell, A. Aarvold, J. O. Smith, A. Briscoe, J. M. Kanczler, K. M. Shakesheff, S. M. Howdle, D. G. Dunlop, R. O. C. Oreffo
A comparison of polymer and polymer–hydroxyapatite composite tissue engineered scaffolds for use in bone regeneration
J. Biomed. Mat. Res., 102 (2014), pp. 2613-2624

[37] S.C. Rizzi, D.J. Heath, A.G. Coombes, N. Bock, M. Textor, S. Downes
Biodegradable polymer/hydroxyapatite composites: surface analysis and initial attachment of human osteoblasts
J. Biomed. Mat. Res., 55 (2001), pp. 475-86

[38] L.D. Silvio, M.J. Dalby, W. Bonfield
Osteoblast Behavior on HAP/PE Composite Surfaces with Different HA Volumes
Biomaterials. 23(2002), pp. 101-107

[39] M. Wang, D. Porter, W. Bonfield
Processing, Characterization, and Evaluation of Hydroxyapatite Reinforced Polyethylene Composites
Brit. Ceram. Trans., 93 (1994), pp. 91-95

[40] D.B. Burr DB
The contribution of the organic matrix to bone's material properties

Bone, 31 (2002), pp. 8-11

[41] S. Viguet-Carrin, P. Garnero, P.D. Delmas

The role of collagen in bone strength

Osteoporos. Int., 17 (2006), pp. 319-336

[42] R.B. Martin, S.T. Lau, P.V. Mathews, V.A. Gibson, S.M. Stover

Collagen fiber organization is related to mechanical properties and remodeling in equine bone. A comparison of two methods

J. Biomech., 29 (1996), pp. 1515-1521

[43] D.A. Wahl, J.T. Czernuszka

Collagen-Hydroxyapatite composites for hard tissue repair

Euro. Cells and Mat., 11 (2006), pp. 43-56

[44] X. Wang, R.A. Bank , J.M. TeKoppele, C.M. Agrawal

The role of collagen in determining bone mechanical properties

J. Orthop. Res., 19 (2001), pp. 1021-1026

[45] M. Jarcho, C.H. Bolen

Hydroxyapatite synthesis and characterization in dense polycrystalline form

J. Mat. Sci., 11 (1976), pp. 2027-2035

[46] H.M. Rietveld

A profile refinement method for nuclear and magnetic structure

J. Appl. Crystallogr., 2 (1969), pp. 65-71

[47] A.C. Larson, R.B.V. Dreele

General Structure Analysis System (GSAS)

Los Alamos National Laboratory Report LAUR, (1994), pp. 86-748

[48] B.H. Toby

EXPGUI a graphical user interface for GSAS

J. Appl. Cryst., 34 (2001), pp. 210-213

[49] ASTM

Standard Test Methods for Plane-Strain Fracture Toughness and Strain Energy Release Rate of Plastic Materials

Designation: D 5045 (1999)

[50] H.G. Tattesall , G. Tappin

The work of fracture and its measurement in metal, ceramics and other materials

J. Mat. Sci., 1 (1966), pp. 296-301

[51] A.T. Sänger, W.F. Kuhs

Structural disorder in Hydroxyapatite

Z. Kristallogr., 199 (1992), pp. 123-148

[52] D. Lahiri, S. Ghosh, A. Agarwal

Carbon nanotube reinforced hydroxyapatite composite for orthopedic application

Mat. Sci. Eng. C , 32 (2012), pp. 1727-1758

[53] C.A. Mitchell, R. Krishnamoorti

Non-isothermal crystallization of in situ polymerized poly (epsilon-caprolactam) functionalized-SWNT nanocomposites

Polymer, 46 (2005), pp. 8796 - 8804

[54] G. Junbo, B. Zhao, M.E. Itkis , E. Bekyarova, H.Hu, V. Kranak , A. Yu, R.C. Haddon

Chemical Engineering of the Single-Walled Carbon Nanotube-Nylon 6 Interface

J. Am. Chem. Soc., 128 (2006), pp. 7492-7496

[55] G. Pezzotti, S. Sakakura

Study of the toughening mechanisms in bone and biomimetic hydroxyapatite materials using Raman microprobe spectroscopy

J. Biomed. Mat., 65 (2003), pp. 229-23665:229-36

[56] G. Pezzotti, A.M.F. Asmus, L.P. Ferroni, S. Miki

In situ polymerization into porous ceramic: a novel route to tough biomimetic materials

J. Mat. Sci.: Mat. in Med., 13 (2002), pp. 783-787

Graphical Abstract